separations

MDPI

Article

Chitosan and Metal Oxide Functionalized Chitosan as Efficient Sensors for Lead (II) Detection in Wastewater

Walid Boultif [1], Charif Dehchar [2,3], Youghourta Belhocine [1], Emna Zouaoui [1,*], Seyfeddine Rahali [4], Salah Eddine Zouari [3], Najoua Sbei [5] and Mahamadou Seydou [6,*]

1 Laboratory of Catalysis, Bioprocess and Environment, Department of Process Engineering, Faculty of Technology, University of 20 August 1955, Skikda 21000, Algeria; w.boultif@univ-skikda.dz (W.B.); y.belhocine@univ-skikda.dz (Y.B.)
2 Laboratoire Croissance et Caractérisation de Nouveaux Semi-Conducteurs, Université Ferhat Abbas, Sétif-1, Setif 19000, Algeria; c.dehchar@univ-skikda.dz
3 Department of Process Engineering, Faculty of Technology, University of 20 August 1955, Skikda 21000, Algeria; zouarisalah23@gmail.com
4 Department of Chemistry, College of Science and Arts, Qassim University, Ar Rass 52719, Saudi Arabia; s.rahali@qu.edu.sa
5 Institute of Nanotechnology, Karlsruhe Institute of Technology, Eggenstein Leopoldshafen, 76344 Karlsruhe, Germany; najwasbei89@hotmail.fr
6 Université Paris Cité, CNRS, ITODYS, F-75013 Paris, France
* Correspondence: e.zouaoui@univ-skikda.dz (E.Z.); mahamadou.seydou@univ-paris-diderot.fr (M.S.)

Abstract: The work presented in this paper describes the preparation and the electrochemical application of functionalized chitosan-entrapped carbon paste electrodes (CH/CPE) for lead ions (Pb^{2+}) detection in industrial wastewater. The chitosan was first functionalized using TiO_2 and CuO, which were both metal oxides that were obtained by extracting it from waste products derived from shrimp shells. The analytical performance of the as-prepared electrodes, CH/CPE, TiO_2-CH/CPE, and NiO-CH/CPE, for the detection of lead (II) was examined using electrochemical impedance spectroscopy (EIS) technique in the 0.1 M KNO_3 electrolyte solution. The effect of experimental conditions, including polarization potential, frequency, and pH, are optimized to maximize the sensitivity of the measurements. The developed impedimetric sensors provided a linear response over a concentration range of 10^{-6} to 10^{-4} M with a detection limit of 3.10^{-7} M based on S/N = 3. The DFT computational analysis demonstrated that chitosan biopolymer possesses the ability to adsorb Pb (II) ions that are present in wastewater. Chitosan and the derivatives of chitosan, have the potential to remove heavy metals from industrial effluent in a manner that is both economical and eco-friendly to the environment. Chitosan is a biopolymer that is abundantly renewable.

Keywords: chitosan; lead (II) detection; metal oxide; sensor; wastewater

Citation: Boultif, W.; Dehchar, C.; Belhocine, Y.; Zouaoui, E.; Rahali, S.; Zouari, S.E.; Sbei, N.; Seydou, M. Chitosan and Metal Oxide Functionalized Chitosan as Efficient Sensors for Lead (II) Detection in Wastewater. *Separations* **2023**, *10*, 479. https://doi.org/10.3390/separations10090479

Academic Editor: Antonio Turco

Received: 30 July 2023
Revised: 27 August 2023
Accepted: 30 August 2023
Published: 31 August 2023

1. Introduction

Lead is a highly toxic metal and a harmful pollutant that affects public health and the environment [1–5]. Due to its toxicity even at low levels, the usage of lead was prohibited or regulated in many industries. However, in some countries, the continued use of lead in paints [6,7], pigments [8], gasoline [9,10], ammunition [11,12], ceramic glazes [13,14], aviation fuel [15], batteries [16], mining [17], smelting [18], and recycling activities [19] is still representing an important environmental pollution and health issue.

As an example, Fe^{3+} plays a key role in several biochemical reactions and is considered a vital element for survival. However, a high accumulation level of Fe^{3+} could result in liver damage, heart diseases, and diabetes.

Indeed, significant amounts of heavy metals such as mercury (Hg) would lead to renal failure, hearing damage, and nerve disorders in the human body. Pb and cadmium (Cd) enter the environment through the metallurgical industry [20,21], burning of fossil fuels [22],

and wastewater releases [23,24]. Lead is not biodegradable and resists corrosion [25], leading to its accumulation in air, water, and soil [26]; therefore, the development of reliable methods to detect and remove lead is of utmost importance [27–34]. However, the direct detection in the samples of trace-heavy metals such as lead (Pb) and cadmium (Cd) is a difficult task, mainly due to their very low concentrations, often below the detection limit of available techniques [35]; including spectroscopic methods, such as atomic emission spectroscopy (AES), atomic absorption spectroscopy (AAS), chromatography methods, etc. However, these methods have limitations for their widespread applications due to their high cost, time consumption, and sophisticated operations.

Nowadays, the development of advanced technologies, abundant unique sensing platforms based on MS, colorimetry, electrochemistry, surface-enhanced Raman scattering (SERS), and fluorescence have been reported to detect trace metal ions.

The reported results showed that MS and SERS with ultrahigh sensitivity gave exact molecular information. The colorimetric and fluorescent sensors allow simply and intuitively observing the changes generated by the target metal ions. Furthermore, electrochemical sensors are suitable for simultaneous detection of various metal ions due to their distinctive and fast responses to different metal ions. Moreover, in order to enhance the sensitivity and selectivity of metal–ion sensors, nanomaterials have been extensively applied in sensor constructions, such as noble metal nanoparticles, porous nanomaterials, semiconductors, etc.

In recent decades, the use of metal oxide has been grown in different applications; for example, the perovskite oxides have been used as a catalyst to produce green hydrogen, which was reported by Daqin Guan and co-workers [36]. Similarly, Guan et al. reported that the tensile-strained RuO_2 has been used as a catalyst for the proton-exchange membrane in water electrolysis [37]. Recently in 2023, transition metal oxides (TMOs) have been used in Li-S battery application which contribute to the high-rate and long-durability of the battery [38].

The monitoring of lead contamination levels in wastewaters is crucial for the effective control of lead pollution [38]. The World Health Organization (WHO) recommends maintaining the concentration of lead as low as possible (the safe limit of Pb content in wastewater is 0.01 ppm) [39]. Several methods have been developed to remove lead from wastewater, such as ion exchange [40–42], adsorption [43–47], reverse osmosis [48–50], precipitation [51–53], electrocoagulation [54–58], and electrodialysis [59,60].

The detection of lead in wastewater can be achieved using a variety of analytical devices such as chromatographs and spectrophotometers [61–63], but they are generally complex, expensive, and often difficult to use—these disadvantages show the need for an alternative approach to classical instruments [64,65].

Chemical sensors represent a powerful analytical tool for simple, inexpensive, reliable, rapid, and selective detection of heavy metals [66–70]. Currently, chemical sensors are widely used in various applications that include biomedical instrumentation, detection of industrial emissions, electrochemical sensing devices, environmental pollution, and water quality monitoring [71,72].

Particularly in recent times, there has been a lot of interest in sensors that are based on electrochemistry because of their potential as on-site environmental pollution monitors. The creation of an electrochemical sensor needs the optimization of two different components: a selective part and a transducer system. Among different transduction techniques, electrochemical impedance spectroscopy is considered as one of the most versatile and powerful methods for determining the electrical properties occurring at the sensor–analyte interface [73–75].

The development of theoretical approaches used to investigate the interaction properties for the detection of environmental pollution has been discussed in a series of papers. Currently, the density–functional theory (DFT) is largely used in computational approaches to confirm and complete experimental findings, and specifically to describe the interaction mechanism between the pollutant and the developed system.

In this study, we investigated the behavior of developed electrochemical sensors based on chitosan and functionalized chitosan by TiO_2 and NiO for the detection of lead ions found in industrial wastewater. Chitosan and its derivatives, as biodegradable and non-toxic natural polymers, may exhibit interesting sensing properties.

2. Materials and Methods

2.1. Chemicals and Reagents

Chitosan is extracted from shrimp Parapenaeuslongirostris shells (Figure 1a), collected from local fish restaurants in Skikda City (Algeria), by a chemical process following the protocol of Benhabiles et al. [76]. Chemicals used for the chitosan preparation process are hydrochloric acid (HCl 36%), sodium hydroxide (NaOH, 99%), and hydrogen peroxide (H_2O_2, 30%) (purchased from Prolabo). Acetic acid (CH_3CO_2H), tin oxide (TiO_2), and nickel (II) oxide (purchased from Sigma–Aldrich) were used for the functionalization of chitosan. In order to make the carbon pastes, high-quality graphite powder with a mesh size of 325, supplied by Asbury Carbons, and paraffin oil with a purity level of 99% were required as ingredients. There was no treatment of any of the compounds before usage. In each of the tests, distilled water was utilized throughout the preparation and analysis processes.

(**a**) (**b**)

Figure 1. Shrimp of Parapenaeuslongirostris: (**a**) shells and (**b**) powder.

2.2. Preparation of Chitosan

The shrimp wastes were prepared for use by first having their legs and antennae removed and were then washed multiple times in warm water (70 °C) to eliminate any organic residues, and at last were air-dried for an entire night (Figure 1a). In the end, the waste samples were reduced to a powdery consistency by being ground in a porcelain mortar and pestle (Figure 1b).

The preparation process involves four steps: first, deproteinization is achieved in sodium hydroxide (2.5 N, NaOH) solution at a solvent to solid ratio (v/w) of 10/1 mL/g at 75 °C during 6 h. The product is then decanted under vacuum, washed thoroughly with distilled water until the pH reaches a neutral value (pH = 7) and is oven-dried at 80 °C for 3 h. The second step consists of demineralization by acid treatment to eliminate calcium carbonate and calcium phosphate naturally present in shrimp shells [77]. Hydrochloric acid of 1.7 N is used with a solvent to solid ratio of 10/1 mL/g at ambient temperature during the 6 h. The final product, chitin, is given a quick rinse in running water before being dried in an oven at 80 degrees Celsius for 3 h. The subsequent procedure is referred to as "decolorization," and its purpose is to remove the pigments from the chitin using reagents, such as ether, ethanol, sodium hypochlorite, or hydrogen peroxide. In this study, a 30% concentration of hydrogen peroxide of was used at ambient temperature for 10 min. After that, the samples were washed thoroughly with tap water to remove any residual impurities and oven-dried at 80 °C for 3 h. The last step was deacetylation by concentrated sodium hydroxide (50%) solution with a solvent to solid ratio of 10/1 mL/g at ambient

temperature for 48 h. By removing the acetyl group from the chitin in this stage (Figure 2), the goal was to transform the chitin into chitosan. Chitosan, the product that was obtained, was put through a filter, washed with distilled water until the filtrate became neutral, and then oven-dried at a temperature of 50 °C overnight.

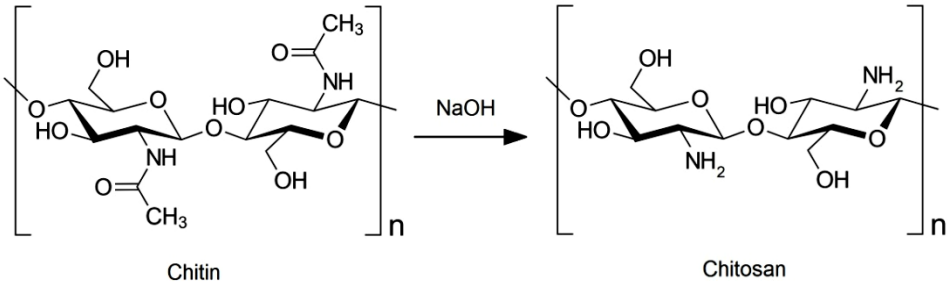

Figure 2. Conversion of chitin to chitosan by alkaline deacetylation.

2.3. Preparation of Functionalized Chitosan

Functionalization of chitosan aims to improve its properties, including electronic, mechanical, and electrochemical properties, to develop new materials for diverse applications [78]. In general, this functionalization is achieved by acid treatments, as chitosan is only soluble in acidic solutions and does not disperse easily in water [79]. In this study, chitosan was placed in 200 mL of 5% (*v*/*v*) acetic acid solution for 24 h to form a homogenous suspension. The experiments were carried out at room temperature (~22 °C) with constant stirring (200 rpm). Next, 10% (*w*/*v*) of active substance X (X = TiO_2, NiO) was gradually added to mix with the suspension under constant stirring. Duration of the experiment was 24 h at ambient temperature. The obtained mixture was then washed several times by distilled water, filtered under vacuum, and dried in an oven at 100 °C.

The choice of the two metal oxides (TiO_2 and NiO) for functionalizing chitosan was based on their distinct properties, such as binding affinity with surfaces capable of undergoing complexation, ion exchange, and electrostatic interactions with lead ions. Furthermore, their catalytic abilities enable them to catalyze redox reactions involving lead ions, leading to amplified signals in electrochemical sensing methods. Additionally, their biocompatibility and chemical stability make them suitable for integration with chitosan without compromising the composite's overall properties.

2.4. Preparation of Chitosan Modified Electrodes

A carbon paste electrode (CPE) was chosen to prepare our functionalized chitosan-based electrodes, as it is simple to manufacture and suitable for preparing modified electrodes with admixtures of different substances; thus, giving the material certain characteristic properties [80]. The electrodes were prepared by mixing a desired weight (20%) of functionalized chitosan and 70% of selected carbon material (graphite powder) with paraffin oil, as a binder, using an agate mortar and pestle for 30 min until a homogeneous mixture was obtained. This ratio was carefully chosen to achieve an optimal balance between the enhanced binding properties of functionalized chitosan and the electrical conductivity of graphite powder.

The synthesized mixture was then introduced into a PVC tube of an appropriate length of 12 cm. Electrical contact was established via passing a thin copper wire from the opposite end through the paste. The outer surfaces of the electrodes were polished with alumina to remove the excess of solidified material and achieve a flat surface. After the electrodes were polished, they were thoroughly rinsed with distilled water and air-dried.

2.5. Fourier Transforms Infrared Spectroscopy (FTIR)

The degree of N-deacetylation (DD) of chitosan samples was determined by the method of Sabnis and Block [81] using FTIR spectroscopy. The spectra were obtained using

a Perkin Elmer 1600 spectrometer from the 4000 to 400 cm^{-1} frequency range. The DD was calculated using the equation proposed by Baxter et al. [82]:

$$DD = 100 - [100 \times (A1655/A3450)/1.33] \quad (1)$$

where DD is N-deacetylation degree and A1655 and A3450 are the absorbance band maxima of the chitosan infrared spectrum at 1655 cm^{-1} of the amide-I band and 3450 cm^{-1} of the hydroxyl band, respectively. The factor 1.33 denotes the value of the ratio A1655/A3450 for fully N-acetylated chitosan [83,84].

2.6. Electrochemical Measurements

Electrochemical impedance spectroscopy (EIS) measurements for the detection of lead (II) on the prepared chitosan-based electrodes were performed in a conventional three-electrode system at room temperature. A platinum (Pt) wire was used as counter electrode (CE), and a saturated calomel electrode (SCE) was used as the reference electrode (RE). All potentials are referred to this electrode. A Voltalab PGZ 301 potentiostat was used to run the experiments.

The working electrode (WE) was incubated for 10 min; then, it was washed and placed in the electrochemical cell containing 0.1 M potassium nitrate (KNO_3) as the supporting electrolyte.

3. Results and Discussion

3.1. FTIR Analysis

FTIR is the most suitable technique for a quick and simple characterization of DD of chitosan. This parameter is extremely important as it influences the properties of the macromolecular chains of the polymers and their behavior in solution, namely the solubility of the chitosan, the flexibility of the macromolecular chains, and the polymer conformation. Figure 3 depicts the infrared spectrum of the chitosan sample. It displays a series of bands: the peak noticed at 1555 cm^{-1} corresponds to N–H bending of the secondary amide II band of –CONH– whereas the amide I band resulting from hydrogen and hydroxyl interactions (due to the deacetylation of chitin) is observed at 1655 cm^{-1}. Small peaks around 2900 cm^{-1} are assigned to the $–CH_2–$ and $–CH_3$ groups. –OH, stretching vibrations of water, and hydroxyls as well as –NH stretching vibrations of free amino groups, are observed at 3100–3500 cm^{-1}. Using the Baxter equation (Equation (1)), the DD of the produced chitosan was found to be 53.33%.

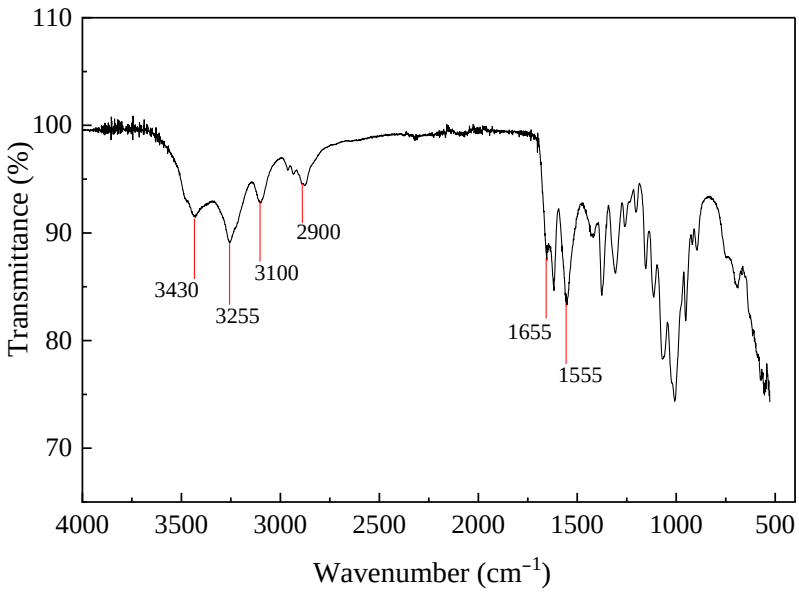

Figure 3. FTIR spectrum of prepared chitosan.

3.2. Detection of Pb (II)

The electrochemical impedance spectroscopy (EIS) technique was used to investigate the electrochemical detection of lead. The optimal experimental conditions, in terms of polarization potential, frequency, and pH, were first determined. Indeed, these parameters are known to have a significant effect on the response of impedimetric sensors.

Figure 4a shows the impedance spectra in the Nyquist plots of the CH/CPE electrode at different potentials (−100, −200, and −400 mV) over a range of frequency from 0.1 Hz to 100 kHz and a sinusoidal excitation signal amplitude of 10 mV. At negative voltages, there is a clear decrease in total impedance. The Warburg straight line at the low-frequency side is reduced as the potential decreases, disappearing at −400 mV and being replaced by a well-defined semicircle. This means that at this potential, the charge–transfer resistance is lower and mass transport has no significant effect on the electrode response. A very similar behavior has been obtained with the TiO_2-CH/CPE and NiO-CH/CPE electrodes; hence, the polarization potential of −400 mV and frequency range from 0.1 Hz to 100 kHz were retained for the rest of this study.

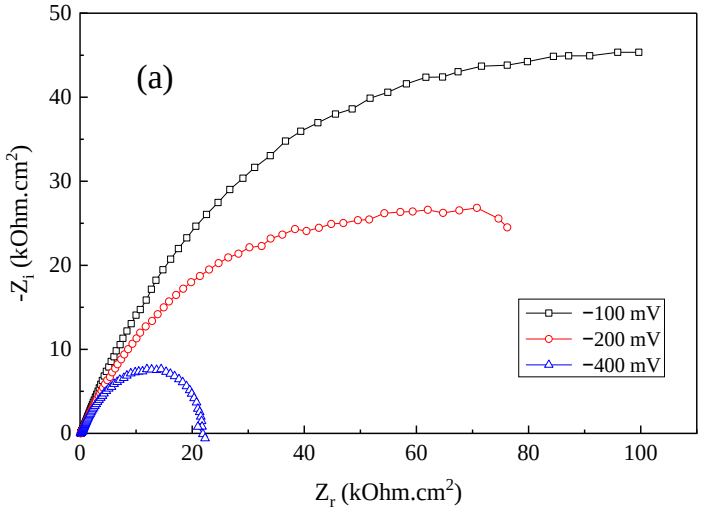

(**a**)

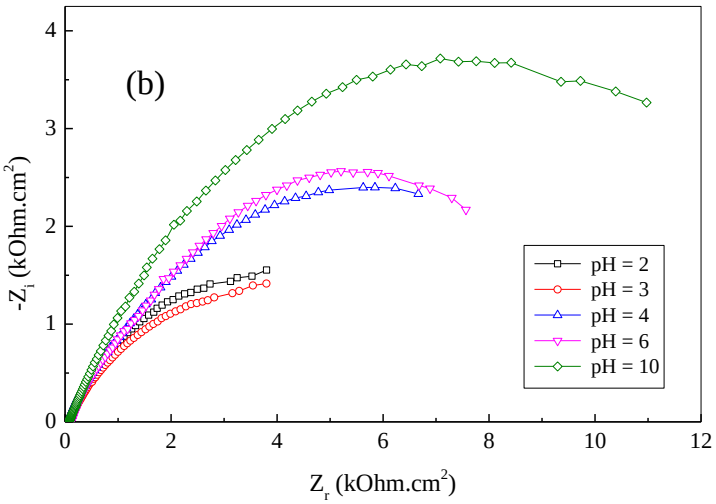

(**b**)

Figure 4. Impedance spectra in Nyquist representation of CH/CPE electrode in 0.1 M KNO_3 electrolyte: (**a**) at different polarization potentials and (**b**) at different pH values.

Figure 4b shows impedance spectra of the CH/CPE electrode recorded at different pH values: 2, 3, 4, 6 and 10. The pH was adjusted by adding KOH and HCl to the electrolyte. As can be seen, the electrode showed very different responses depending on the pH value. The best response, in terms of lower charge–transfer resistance, was obtained at pH = 6; therefore, this value of pH was chosen for further study.

The electrochemical response of the CH/CPE, TiO_2-CH/CPE and NiO-CH/CPE electrodes for the detection of lead ions (Pb^{2+}) was examined using EIS measurements in 0.1 M KNO_3 electrolyte in the presence of different concentrations of the target analyte.

Figure 5a–c show the Nyquist plots of the impedance spectra corresponding to the three electrodes. A sharp decrease in total impedance, for all three cases, is clearly seen after addition of Pb^{2+} ions, indicating a good sensitivity of the developed electrodes to changes in analyte concentration.

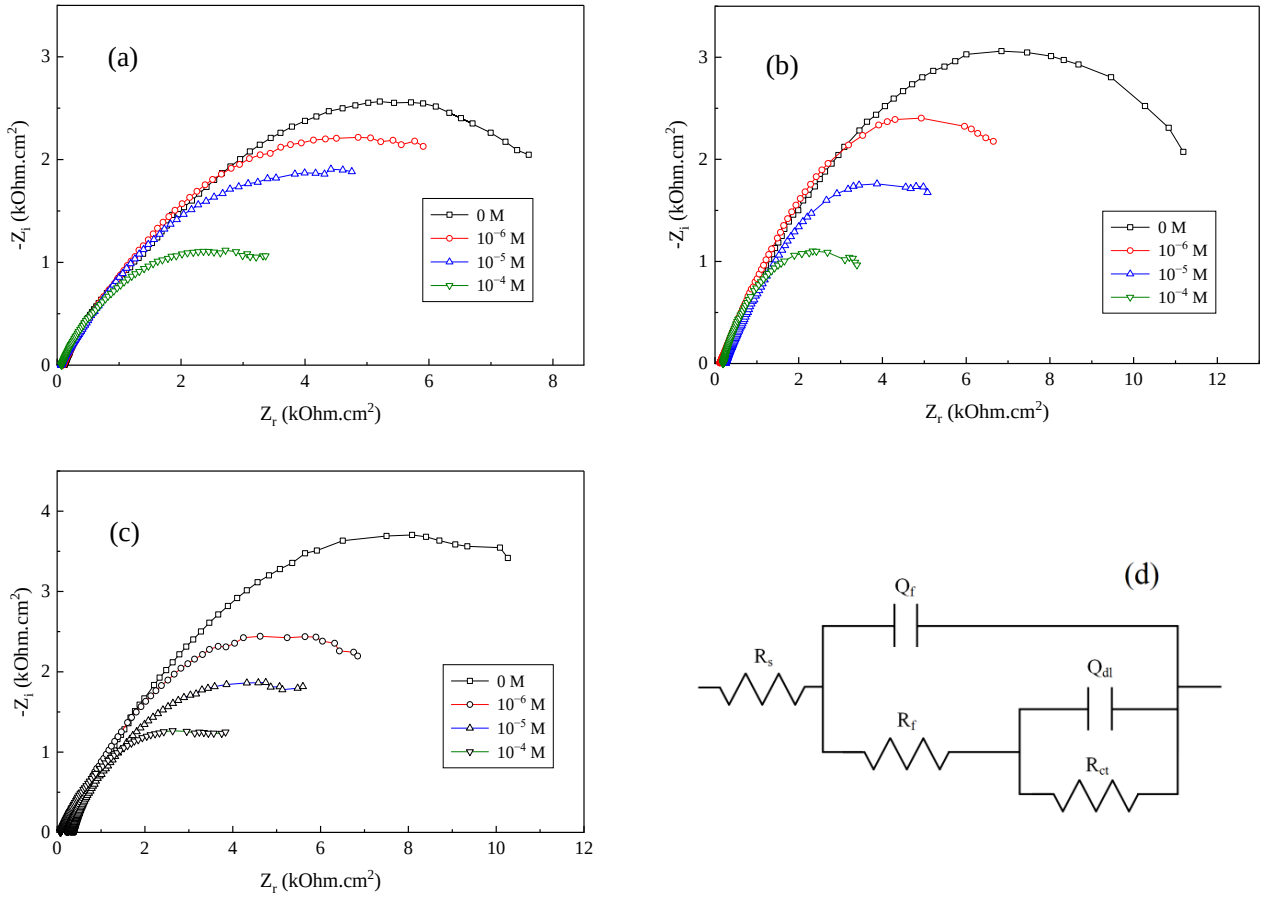

Figure 5. Impedance spectra in the Nyquist diagrams in 0.1 M KNO_3 in the presence of different concentrations of Pb^{2+} recorded on: (**a**) CH/CPE, (**b**) TiO_2-CH/CPE, and (**c**) NiO-CH/CPE electrodes. (**d**) Equivalent electric circuit proposed to fit the impedance spectra.

The impedance spectra were fitted using the equivalent circuit shown in Figure 5d. The given model is a combination of three parts. The first part is a series resistance of the electrolyte solution, R_s. The second part at high frequency sides, which is attributed to the electrode/film interface, is reproduced by a film capacitance, Q_f, and a film resistance, R_f. The third part at the low frequency, which is attributed to the film/electrolyte interface, is reproduced by a charge–transfer resistance, R_{ct}, in parallel with a double-layer capacitance, Q_{dl}.

To evaluate the performance of the electrodes for lead ions determination, the evolution of charge–transfer resistance, R_{ct}, is used. The fitted values of R_{ct} are summarized in Table 1.

Table 1. The values of the R_{ct} in equivalent circuit fitted in the Nyquist plots of Figure 5 as a function of Pb^{2+} concentration.

$[Pb^{2+}]$	CH/CPE	TiO_2-CH/CPE	NiO-CH/CPE
	R_{ct} (Ohm.cm^2)	R_{ct} (Ohm.cm^2)	R_{ct} (Ohm.cm^2)
0	11,476	7032	15,385
10^{-6}	10,422	4811	9744
10^{-5}	8435	4692	8585
10^{-4}	4703	4610	5423

Table 1 reveals that the Rct gradually reduces as the concentration of Pb^{2+} ions in the solution increases; hence, this suggests that the charge–transfer is improved when there is a larger concentration of Pb^{2+} ions in the solution. This can be seen for all three electrodes. In fact, the current flow increases as the ionic concentration rises, while the charge–transfer resistance falls. This is because there are more ions participating in the electric conduction process as the ionic concentration rises. The sensing performance of the electrodes is figured out by first plotting calibration curves, which are performed with the help of the correlation that exists between the amount of the ions present in the solution and the charge–transfer resistance. The calibration curves of the sensors, shown in Figure 6, present the variation of charge–transfer resistance, $R_{ct0} - R_{ct}$, versus the added concentration of Pb^{2+} ions where R_{ct0} is the charge–transfer resistance of the electrolyte solution without Pb^{2+} ions.

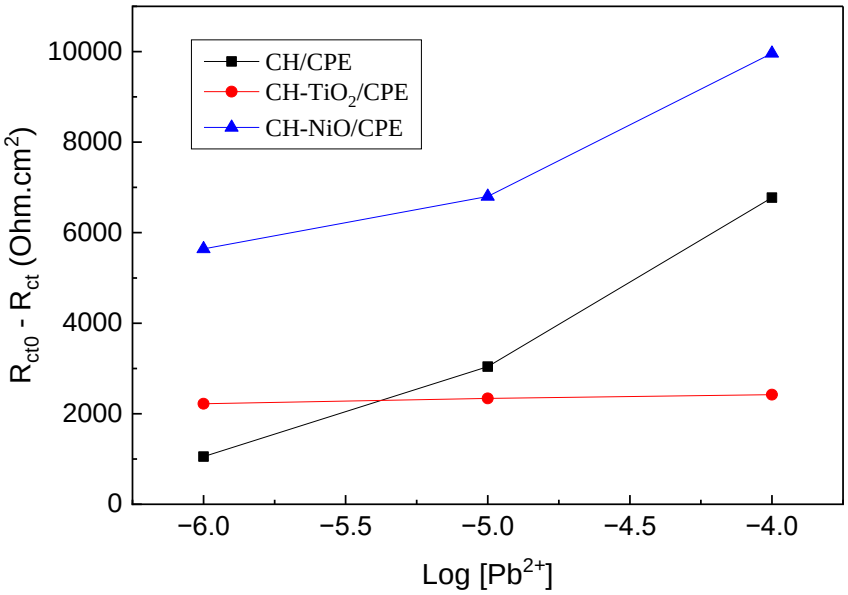

Figure 6. Calibration curves of the sensors: $R_{ct0} - R_{ct}$ versus log ($[Pb^{2+}]$/M).

These results indicate that functionalized chitosan demonstrates improved performance in terms of –charge–transfer compared to non-functionalized chitosan. This enhancement becomes particularly pronounced in the low lead ion concentration range ($<10^{-5}$ M) for TiO_2, while the influence of NiO addition can be observed across all tested concentration ranges.

The limit of detection (LOD) was determined from the formula $3\sigma/s$ where σ is the standard deviation of the intercept and s is the slope of the calibration curve.

In order to evaluate the analytical performance of the impedimetric sensors that were constructed, a comparison was made with the analytical performance of other sensors from the published literature that were utilized for the measurement of Pb^{2+} ions. As can be observed in Table 2, not only did our sensors have a straightforward preparation procedure and a low cost of manufacture, but they also displayed a wide linear range and a low detection limit.

Table 2. Comparison of various electrode materials for Pb^{2+} sensing.

Electrode Material	Analytical Method	Linear Range (M)	LOD (M)	Reference
Poly (dimethylsiloxane) microchip	Indirect amperometry	5.10^{-6} to10^{-3}	$1.3.10^{-6}$	[85]
Poly (1,8-diaminonaphthalene) modified CPE	Differential pulse voltammetry	2.10^{-7} to 10^{-5}	$1.4.10^{-7}$	[86]
ZYMCPE on ITO	Cyclic voltammetry	$2.5.10^{-8}$ to 10^{-7}	$1.7.10^{-8}$	[87]
Bismuth/glassy carbon composite	Anodic stripping voltammetry	5.10^{-7} to 10^{-7}	10^{-8}	[88]
Antimony film electrode	Anodic stripping voltammetry	10^{-7} to 7.10^{-7}	4.10^{-9}	[89]
CH/CPE, TiO_2-CH/CPE, NiO-CH/CPE	EIS	10^{-6} to 10^{-4}	3.10^{-7}	This work

3.3. Selectivity Study

The selectivity of the developed impedimetric sensors toward Pb^{2+} ions was tested in the presence of Cd^{2+} interfering ions at different concentrations. The typical Nyquist plots of impedance spectra of Pb^{2+} solution in the absence and presence of Cd^{2+} are shown in Figure 7a–c.

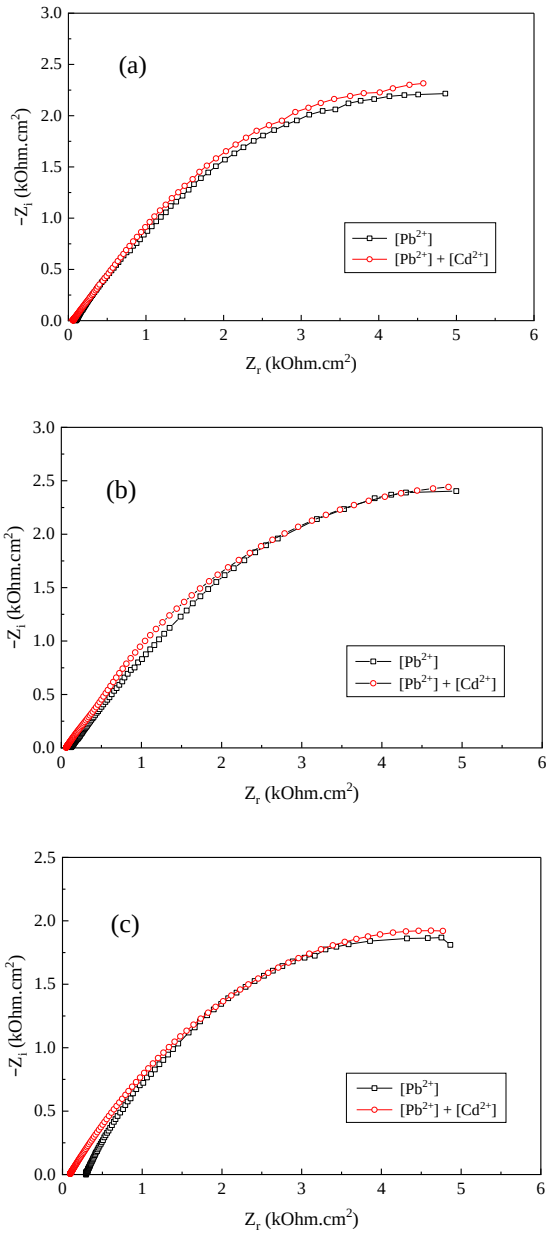

Figure 7. Impedance spectra of Pb^{2+} solution in the absence and presence of Cd^{2+} in 0.1 M KNO_3 electrolyte solution recorded on: (**a**) CH/CPE, (**b**) TiO_2-CH/CPE, and (**c**) NiO-CH/CPE electrodes.

The impedance spectra of all three electrodes in the presence of Cd^{2+} ions did not show any noticeable change in responses, which indicates that the electrodes have a good selectivity to the analyte of interest.

3.4. DFT-D3 Calculations of Intermolecular Interactions

We carried out a computer analysis making use of DFT calculations in order to verify the outcomes that were achieved. Using the periodic DFT approach that is included in the Vienna Ab initio Simulation Package (VASP 5.4.1), an investigation into the selectivity of chitosan for the adsorption of Pb^{2+} and Cd^{2+} ions was carried out. [90]. The generalized gradient approximation (GGA) was used with the Perdew−Burke−Ernzerhof (PBE) function [91]. The cutoff energy for the plane wave basis set used in this study is 500 eV. The convergence criteria for the geometry optimization were 2.0×10^{-4} Å for maximum displacement and 0.05 eV/Å for maximum force. The Monkhorst−Pack scheme is used to generate a grid of ($3 \times 3 \times 1$) k-points. The dispersion effect is added using the Grimme approach [92]. The unit cell used in this study consists of 12 carbon, 8 oxygen, 22 hydrogen and 2 nitrogen atoms (Figure 8a). The slab model was employed where the vacuum size of 30 Å was set along the *z*-axis to avoid the heavy metal interacting with its nearby images.

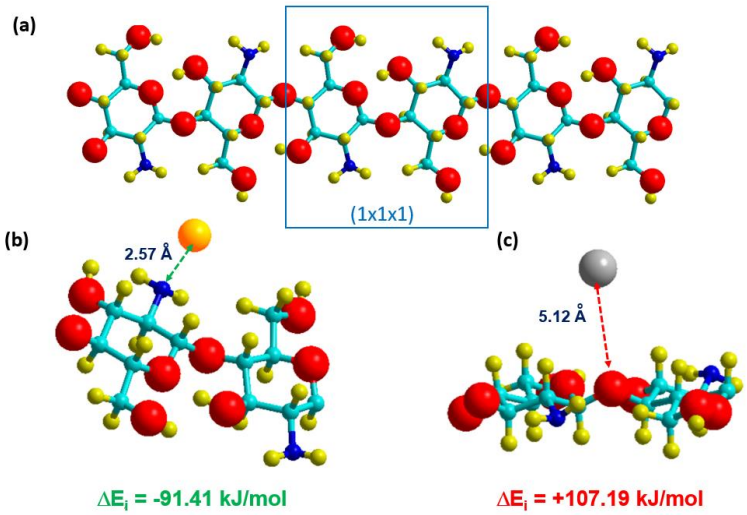

Figure 8. Optimized structures of the unit cell of chitosan (**a**), the Pb^{2+}-chitosan complex (**b**), and the Cd^{2+}-chitosan complex (**c**).

The different possible adsorption sites of lead and cadmium cations were optimized. The more stable optimized structures are presented in Figure 8b,c. The interaction energy (ΔE_i) were then calculated using the following equation:

$$\Delta E_i = E_{MC}{}^{2+} - (E_C + E_M{}^{2+})$$

where $E_{MC}{}^{2+}$ is the total energy of the heavy metal cations adsorbed on chitosan molecule, E_C is the total energy of chitosan, and $E_M{}^{2+}$ is the energy of isolated cations. Therefore, negative interaction energy suggest that the adsorption process is exothermic, and that the detection of metal cations leads to stable configurations. On the other hand, positive adsorption energy suggest that unstable configurations may emerge from the detection of metal cations. Figure 8b,c present the geometries that are the most stable for the various complexes formed by lead and cadmium ions that are adsorbed on chitosan, along with the energy that are associated with those geometries. Data gathered in Figure 8 indicate that the Pb^{2+}/chitosan complexation is an exothermic process, as calculated adsorption energy is negative (−91.41 kJ/mol), and that the interaction with Cd^{2+} is unfavorable, as the interaction energy is positive (107.19 kJ/mol). Therefore, the chitosan is only capable of adsorbing lead ions (Pb^{2+}) when exposed to wastewater that also includes cadmium.

4. Conclusions

An environmentally friendly method that is based on the valorization of chitosan recovered from discarded shrimp shells has enabled the development of a straightforward and economical method for the fabrication of impedimetric sensors for the detection of the lead ions Pb^{2+}. In this study, we demonstrated that the extracted chitosan could be functionalized with various metal oxides (TiO_2 and NiO), which would then result in the production of active materials. In addition, we demonstrated that electrochemical impedance spectroscopy is a method that is both suitable and effective for the analytical sensing of lead (II) ions, even at extremely low concentrations. The results of the DFT show that there is a powerful contact between the lead ion and the nitrogen atom of the chitosan molecule. This association has an adsorption bond length of 2.57 Å and an adsorption energy of −91.41 kJ/mol. The prepared chitosan and functionalized chitosan-based electrodes displayed good analytical performance as impedimetric sensors with a large linear range (10^{-6}–10^{-4} M) and low limit of detection (3.10^{-7} M); hence, they look promising for wastewater monitoring applications.

Author Contributions: Conceptualization, E.Z.; methodology, C.D. and W.B.; software, S.R. and C.D.; validation, Y.B., E.Z., N.S. and M.S.; formal analysis, S.E.Z., W.B. and C.D.; investigation, Y.B., W.B., C.D., M.S., N.S. and S.R.; resources, S.E.Z.; data curation, W.B., C.D., Y.B. and S.R.; writing—original draft preparation, C.D., Y.B., S.R. and W.B.; writing—review and editing, E.Z. and M.S.; visualization, C.D. and S.R.; supervision, E.Z., Y.B. and C.D.; project administration, E.Z. and W.B.; funding acquisition, M.S. All authors have read and agreed to the published version of the manuscript.

Funding: This research received no external funding.

Data Availability Statement: The data presented in this study are available on request from the corresponding author.

Acknowledgments: Quantum chemical calculations were performed using HPC resources from GENCI- [CCRT/CINES/IDRIS] (Grant 2020[A0140807006]).

Conflicts of Interest: The authors declare no conflict of interest.

References

1. Demayo, A.; Taylor, M.C.; Taylor, K.W.; Hodson, P.V. Toxic effects of lead and lead compounds on human health, aquatic life, wildlife plants, and livestock. *CRC Crit. Rev. Environ. Control* **2009**, *12*, 257–305. [CrossRef]
2. Kumar, A.; Kumar, A.; Pinto, M.M.S.C.; Chaturvedi, A.K.; Shabnam, A.A.; Subrahmanyam, G.; Mondal, R.; Gupta, D.K.; Malyan, S.K.; Kumar, S.S.; et al. Lead toxicity: Health hazards, influence on food chain, and sustainable remediation approaches. *Int. J. Environ. Res. Public Health* **2020**, *17*, 2179. [CrossRef]
3. Loh, N.; Loh, H.P.; Wang, L.K.; Wang, M.H.S. Health Effects and Control of Toxic Lead in the Environment. In *Natural Resources and Control Processes*; Wang, L., Wang, M.H., Hung, Y.T., Shammas, N., Eds.; Handbook of Environmental Engineering; Springer: Cham, Switzerland, 2016; Volume 17. [CrossRef]
4. Wani, A.L.; Ara, A.; Usmani, J.A. Lead toxicity: A review. *Interdiscip. Toxicol.* **2015**, *8*, 55–64. [CrossRef]
5. Flora, G.; Gupta, D.; Tiwari, A. Toxicity of lead: A review with recent updates. *Interdiscip. Toxicol.* **2012**, *5*, 47–58. [CrossRef]
6. O'Connor, D.; Hou, D.; Ye, J.; Zhang, Y.; Ok, Y.S.; Song, Y.; Coulon, F.; Peng, T.; Tian, L. Lead-based paint remains a major public health concern: A critical review of global production, trade, use, exposure, health risk, and implications. *Environ. Int.* **2018**, *121*, 85–101. [CrossRef]
7. Gottesfeld, P. Time to ban lead in industrial paints and coatings. *Front. Public Health* **2015**, *3*, 144. [CrossRef]
8. Rosner, D.; Markowitz, G.; Lanphear, B.J. Lockhart Gibson and the discovery of the impact of lead pigments on children's health: A review of a century of knowledge. *Public Health Rep.* **2005**, *120*, 296–300. [CrossRef]
9. Thomas, V.M.; Socolow, R.H.; Fanelli, J.J.; Spiro, T.G. Effects of reducing lead in gasoline: An analysis of the international experience. *Environ. Sci. Technol.* **1999**, *33*, 3942–3948. [CrossRef]
10. Patrick, L. Lead Toxicity, a Review of the Literature. Part I: Exposure, Evaluation and Treatment. *Altern. Med. Rev.* **2006**, *11*, 2–22.
11. Arnemo, J.M.; Andersen, O.; Stokke, S.; Thomas, V.G.; Krone, O.; Pain, D.J.; Mateo, R. Health and environmental risks from lead-based ammunition: Science versus socio-politics. *EcoHealth* **2016**, *13*, 618–622. [CrossRef]
12. Golden, N.H.; Warner, S.E.; Coffey, M.J. A Review and Assessment of Spent Lead Ammunition and Its Exposure and Effects to Scavenging Birds in the United States. In *Reviews of Environmental Contamination and Toxicology*; De Voogt, W., Ed.; Springer: Cham, Switzerland, 2016; Volume 237. [CrossRef]
13. Harris, R.W.; Elsea, W.R. Ceramic glaze as a source of lead poisoning. *J. Am. Med. Assoc.* **1967**, *202*, 544–546. [CrossRef]

14. Dorevitch, S.; Babin, A. Health hazards of ceramic artists. *Occup. Med.* **2001**, *16*, 563–575. [PubMed]
15. Kumar, T.; Mohsin, R.; Ghafir, M.F.A.; Kumar, I.; Wash, A.M. Concerns over use of leaded aviation gasoline (AVGAS) fuel. *Chem. Eng. Trans.* **2018**, *63*, 181–186. [CrossRef]
16. Zhang, J.; Chen, C.; Zhang, X.; Liu, S. Study on the environmental risk assessment of lead-acid batteries. *Procedia Environ. Sci.* **2016**, *31*, 873–879. [CrossRef]
17. Singh, N.; Li, J.H. Environmental impacts of lead ore mining and smelting. *Adv. Mater. Res.* **2014**, *878*, 338–347. [CrossRef]
18. Body, P.E.; Inglis, G.; Dolan, P.R.; Mulcahy, D.E. Environmental lead: A review. *Crit. Rev. Environ. Sci. Technol.* **1991**, *20*, 299–310. [CrossRef]
19. Uzu, G.; Sobanska, S.; Sarret, G.; Sauvain, J.J.; Pradère, P.; Dumat, C. Characterization of lead-recycling facility emissions at various workplaces. Major insights for sanitary risk assessment. *J. Hazard. Mater.* **2011**, *186*, 1018–1027. [CrossRef]
20. Tchounwou, P.B.; Yedjou, C.G.; Patlolla, A.K.; Sutton, D.J. Heavy Metal Toxicity and the Environment. In *Molecular, Clinical and Environmental Toxicology*; Luch, A., Ed.; Experientia Supplementum; Springer: Basel, Switzerland, 2012; Volume 101. [CrossRef]
21. Hambach, R.; Lison, D.; D'Haese, P.C.; Weyler, J.; De Graef, E.; De Schryver, A.; Lamberts, L.V.; van Sprundel, M. Co-exposure to lead increases the renal response to low levels of cadmium in metallurgy workers. *Toxicol. Lett.* **2013**, *222*, 233–238. [CrossRef]
22. Maciejczyk, P.; Chen, L.C.; Thurston, G. The Role of Fossil Fuel Combustion Metals in PM2.5 Air Pollution Health Associations. *Atmosphere* **2021**, *12*, 1086. [CrossRef]
23. Igiri, B.E.; Okoduwa, S.I.R.; Idoko, G.O.; Akabuogu, E.P.; Adeyi, A.O.; Ejiogu, I.K. Toxicity and bioremediation of heavy metals contaminated ecosystem from tannery wastewater: A review. *J. Toxicol.* **2018**, *2018*, 2568038. [CrossRef]
24. Mahmood, A.; Mirza, M.A.; Choudhary, M.A.; Kim, K.H.; Raza, W.; Raza, N.; Lee, S.S.; Zhang, M.; Lee, J.H.; Sarfraz, M. Spatial distribution of heavy metals in crops in a wastewater irrigated zone and health risk assessment. *Environ. Res.* **2019**, *168*, 382–388. [CrossRef] [PubMed]
25. Tylecote, R.F. The behaviour of lead as a corrosion resistant medium undersea and in soils. *J. Archaeol. Sci.* **1983**, *10*, 397–409. [CrossRef]
26. Deng, H.; Ye, Z.H.; Wong, M.H. Accumulation of lead, zinc, copper and cadmium by 12 wetland plants species thriving in metal contaminated sites in China. *Environ. Poll.* **2004**, *132*, 29–40. [CrossRef] [PubMed]
27. Zulfiqar, U.; Farooq, M.; Hussain, S.; Maqsood, M.; Hussain, M.; Ishfaq, M.; Ahmad, M.; Anjum, M.Z. Lead toxicity in plants: Impacts and remediation. *J. Environ. Manag.* **2019**, *250*, 109557. [CrossRef] [PubMed]
28. Pyrzynska, K. Recent Applications of Carbon Nanotubes for Separation and Enrichment of Lead Ions. *Separations* **2021**, *10*, 152. [CrossRef]
29. Al-Rashdi, B.; Somerfield, C.; Hilal, N. Heavy metals removal using adsorption and nanofiltration techniques. *Sep. Purif. Rev.* **2011**, *40*, 209–259. [CrossRef]
30. Khulbe, K.C.; Matsuura, T. Removal of heavy metals and pollutants by membrane adsorption techniques. *Appl. Water Sci.* **2018**, *8*, 19. [CrossRef]
31. Yadanaparthi, S.K.R.; Graybill, D.; von Wandruszka, R. Adsorbents for the removal of arsenic, cadmium, and lead from contaminated waters. *J. Hazard. Mater.* **2009**, *171*, 1–15. [CrossRef]
32. Karić, N.; Maia, A.S.; Teodorović, A.; Atanasova, N.; Langergraber, G.; Crini, G.; Ribeiro, A.R.; Đolić, M. Bio-waste valorisation: Agricultural wastes as biosorbents for removal of (in) organic pollutants in wastewater treatment. *Chem. Eng. J. Adv.* **2022**, *9*, 100239. [CrossRef]
33. Fu, F.; Wang, Q. Removal of heavy metal ions from wastewaters: A review. *J. Environ. Manag.* **2011**, *92*, 407–418. [CrossRef]
34. Ali, I.H.; Bani-Fwaz, M.Z.; El-Zahhar, A.A.; Marzouki, R.; Jemmali, M.; Ebraheem, S.M. Gum Arabic-Magnetite Nanocomposite as an Eco-Friendly Adsorbent for Removal of Lead(II) Ions from Aqueous Solutions: Equilibrium, Kinetic and Thermodynamic Studies. *Separations* **2021**, *8*, 224. [CrossRef]
35. Li, P.H.; Li, Y.X.; Li, S.H.; Jiang, S.S.; Guo, M.; Liu, Z.; Huang, J.H.; Yang, X.J.; Chen, M. Sensitive and interference-free electrochemical determination of Pb(II) in wastewater using porous Ce-Zr oxide nanospheres. *Sens. Actuators B Chem.* **2018**, *257*, 1009–1020. [CrossRef]
36. Guan, D.; Xu, H.; Zhang, Q.; Huang, Y.C.; Shi, C.; Chang, Y.C.; Xu, X.; Tang, J.; Gu, Y.; Pao, C.W.; et al. Identifying a universal activity descriptor and a unifying mechanism concept on perovskite oxides for green hydrogen production. *Adv. Mater.* **2023**, *2023*, 2305074. [CrossRef]
37. Huang, B.; Xu, H.; Jiang, N.; Wang, M.; Huang, J.; Guan, L. Tensile-Strained RuO2 Loaded on Antimony-Tin Oxide by Fast Quenching for Proton-Exchange Membrane Water Electrolyzer. *Adv. Sci.* **2022**, *9*, 2201654. [CrossRef] [PubMed]
38. Xiao, W.; Kiran, G.K.; Yoo, K.; Kim, J.H.; Xu, H. The Dual-Site Adsorption and High Redox Activity Enabled by Hybrid Organic-Inorganic Vanadyl Ethylene Glycolate for High-Rate and Long-Durability Lithium–Sulfur Batteries. *Small* **2023**, *19*, 2206750. [CrossRef] [PubMed]
39. Kinuthia, G.K.; Ngure, V.; Beti, D.; Lugalia, R.; Wangila, A.; Kamau, L. Levels of heavy metals in wastewater and soil samples from open drainage channels in Nairobi, Kenya: Community health implication. *Sci. Rep.* **2020**, *10*, 8434. [CrossRef]
40. Lalmi, A.; Bouhidel, K.-E.; Sahraoui, B.; el Houda Anfif, C. Removal of lead from polluted waters using ion exchange resin with $Ca(NO_3)_2$ for elution. *Hydrometallurgy* **2018**, *178*, 287–293. [CrossRef]
41. Murray, A.; Örmeci, B. Use of polymeric sub-micron ion-exchange resins for removal of lead, copper, zinc, and nickel from natural waters. *J. Environ. Sci.* **2019**, *75*, 247–254. [CrossRef]

42. Rao, K.S.; Dash, P.K.; Sarangi, D.; Chaudhury, G.R.; Misra, V.N. Treatment of wastewater containing Pb and Fe using ion-exchange techniques. *J. Chem. Technol. Biotechnol.* **2005**, *80*, 892–898. [CrossRef]
43. Raghavendra, N.; Maruthi, N.; Hublikar, L.V.; Koujalagi, S.B.; Prabhu, S.; Mahale, N. Evaluation of PANI-Averraoha bilimbi leaves activated carbon nanocomposite for Cd^{2+} and Pb^{2+} removal from wastewater. *J. Indian Chem. Soc.* **2023**, *100*, 100872. [CrossRef]
44. Kumar, P.S. Adsorption of lead(II) ions from simulated wastewater using natural waste: A kinetic, thermodynamic and equilibrium study. *Environ. Prog. Sustain. Energy* **2014**, *33*, 55–64. [CrossRef]
45. Chauhan, D.; Sankararamakrishnan, N. Highly enhanced adsorption for decontamination of lead ions from battery wastewaters using chitosan functionalized with xanthate. *Bioresour. Technol.* **2008**, *99*, 9021–9024. [CrossRef] [PubMed]
46. Hoang, M.T.; Pham, T.D.; Nguyen, V.T.; Nguyen, M.K.; Pham, T.T.; van der Bruggen, B. Removal and recovery of lead from wastewater using an integratedsystem of adsorption and crystallization. *J. Clean. Prod.* **2019**, *213*, 1204–1216. [CrossRef]
47. Rahali, S.; Aissa, M.A.B.; Modwi, A.; Said, R.B.; Belhocine, Y. Application of mesoporous CaO@g-C_3N_4 nanosorbent materials for high-efficiency removal of Pb (II) from aqueous solution. *J. Mol. Liq.* **2023**, *379*, 121594. [CrossRef]
48. Bartels, C.R.; Wilf, M.; Andes, K.; Iong, J. Design considerations for wastewater treatment by reverse osmosis. *Water Sci. Technol.* **2005**, *51*, 473–482. [CrossRef] [PubMed]
49. Thaçi, B.S.; Gashi, S.T. Reverse osmosis removal of heavy metals from wastewater effluents using biowaste materials pretreatment. *Pol. J. Environ. Stud.* **2019**, *28*, 337–341. [CrossRef]
50. Trishitman, D.; Cassano, A.; Basile, A.; Rastogi, N.K. Reverse osmosis for industrial wastewater treatment. In *Current Trends and Future Developments on (Bio-) Membranes*; Elsevier: Amsterdam, The Netherlands, 2020; pp. 207–228. [CrossRef]
51. Gopalratnam, V.C.; Bennett, G.F.; Peters, R.W. The simultaneous removal of oil and heavy metals from industrial wastewater by joint precipitation and air flotation. *Environ. Prog.* **1988**, *7*, 84–92. [CrossRef]
52. Matlock, M.M.; Howerton, B.S.; Atwood, D.A. Chemical precipitation of lead from lead battery recycling plant wastewater. *Ind. Eng. Chem. Res.* **2002**, *41*, 1579–1582. [CrossRef]
53. Chen, Q.; Yao, Y.; Li, X.; Lu, J.; Zhou, J.; Huang, Z. Comparison of heavy metal removals from aqueous solutions by chemical precipitation and characteristics of precipitates. *J. Water Process Eng.* **2018**, *26*, 289–300. [CrossRef]
54. Butler, E.; Hung, Y.T.; Yeh, R.Y.L.; Al Ahmad, M.S. Electrocoagulation in wastewater treatment. *Water* **2011**, *3*, 495–525. [CrossRef]
55. Oncel, M.S.; Muhcu, A.; Demirbas, E.; Kobya, M. A comparative study of chemical precipitation and electrocoagulation for treatment of coal acid drainage wastewater. *J. Environ. Chem. Eng.* **2013**, *1*, 989–995. [CrossRef]
56. Shahedi, A.; Darban, A.K.; Taghipour, F.; Jamshidi-Zanjani, A. A review on industrial wastewater treatment via electrocoagulation processes. *Curr. Opin. Electrochem.* **2020**, *22*, 154–169. [CrossRef]
57. Mansoorian, H.J.; Mahvi, A.H.; Jafari, A.J. Removal of lead and zinc from battery industry wastewater using electrocoagulation process: Influence of direct and alternating current by using iron and stainless steel rod electrodes. *Sep. Purif. Technol.* **2014**, *135*, 165–175. [CrossRef]
58. SyamBabu, D.; Singh, T.S.A.; Nidheesh, P.V.; Kumar, M.S. Industrial wastewater treatment by electrocoagulation process. *Sep. Sci. Technol.* **2020**, *55*, 3195–3227. [CrossRef]
59. Sadrzadeh, M.; Mohammadi, T.; Ivakpour, J.; Kasiri, N. Separation of lead ions from wastewater using electrodialysis: Comparing mathematical and neural network modeling. *Chem. Eng. J.* **2008**, *144*, 431–441. [CrossRef]
60. Gurreri, L.; Tamburini, A.; Cipollina, A.; Micale, G. Electrodialysis applications in wastewater treatment for environmental protection and resources recovery: A systematic review on progress and perspectives. *Membranes* **2020**, *10*, 46. [CrossRef]
61. Csuros, M.; Csuros, C. *Environmental Sampling and Analysis for Metals*; CRC Press Lewis Publishers: Boca Raton, FL, USA, 2002.
62. Denizli, A.; Say, R.; Arica, Y. Removal of heavy metal ions from aquatic solutions by membrane chromatography. *Sep. Purif. Technol.* **2000**, *21*, 181–190. [CrossRef]
63. Ammann, A.A. Inductively coupled plasma mass spectrometry (ICP MS): A versatile tool. *J. Mass Spectrom.* **2007**, *42*, 419–427. [CrossRef]
64. Eddaif, L.; Shaban, A.; Telegdi, J. Sensitive detection of heavy metals ions based on the calixarene derivatives-modified piezoelectric resonators: A review. *Int. J. Environ. Anal. Chem.* **2019**, *99*, 824–853. [CrossRef]
65. Ajiboye, T.O.; Oyewo, O.A.; Onwudiwe, D.C. Simultaneous removal of organics and heavy metals from industrial wastewater: A review. *Chemosphere* **2021**, *262*, 128379. [CrossRef]
66. Ullah, N.; Mansha, M.; Khan, I.; Qurashi, A. Nanomaterial-based optical chemical sensors for the detection of heavy metals in water: Recent advances and challenges. *TrAC Trends Anal. Chem.* **2018**, *100*, 155–166. [CrossRef]
67. KorentUrek, Š.; Frančič, N.; Turel, M.; Lobnik, A. Sensing heavy metals using mesoporous-based optical chemical sensors. *J. Nanomater.* **2013**, *2013*, 501320. [CrossRef]
68. Raghu, G.K.; Pandurangappa, M. A binderless covalently bulk modified electrochemical sensor: Application to simultaneous determination of lead and cadmium at trace level. *Anal. Chim. Acta* **2012**, *728*, 9–17. [CrossRef]
69. Hasan, M.N.; Salman, M.S.; Islam, A.; Znad, H.; Hasan, M.M. Sustainable composite sensor material for optical cadmium (II) monitoring and capturing from wastewater. *Microchem. J.* **2021**, *161*, 105800. [CrossRef]
70. Shahat, A.; Hassan, H.M.; Azzazy, H.M.; El-Sharkawy, E.; Abdou, H.M.; Awual, M.R. Novel hierarchical composite adsorbent for selective lead (II) ions capturing from wastewater samples. *Chem. Eng. J.* **2018**, *332*, 377–386. [CrossRef]

71. Attia, G.; Rahali, S.; Teka, S.; Fourati, N.; Zerrouki, C.; Seydou, M.; Chehimi, S.; Hayouni, S.; Mbakidi, J.-P.; Bouquillon, S.; et al. Anthracene based surface acoustic wave sensors for picomolar detection of lead ions. Correlation between experimental results and DFT calculations. *Sens. Actuators B Chem.* **2018**, *276*, 349–355. [CrossRef]
72. Attia, G.; Khaldi, Z.; Rahali, S.; Fourati, N.; Zerrouki, C.; Zerrouki, R.; Seydou, M.; Yaakoubi, N.; Chaabane, R.B. Design of surface acoustic wave sensors functionalized with Bisphenol S based molecules for lead ions detection. *Proceedings* **2018**, *2*, 872. [CrossRef]
73. Pan, X.; Zhang, M.; Liu, H.; Ouyang, S.; Ding, N.; Zhang, P. Adsorption behavior and mechanism of acid orange 7 and methylene blue on self-assembled three-dimensional MgAl layered double hydroxide: Experimental and DFT investigation. *Appl. Surf. Sci.* **2020**, *522*, 146370. [CrossRef]
74. Adam, F.A.; Ghoniem, M.G.; Diawara, M.; Rahali, S.; Abdulkhair, B.Y.; Elamin, M.R.; Aissa, M.A.B.; Seydou, M. Enhanced adsorptive removal of indigo carmine dye by bismuth oxide doped MgO based adsorbents from aqueous solution: Equilibrium, kinetic and computational studies. *RSC Adv.* **2022**, *12*, 24786–24803. [CrossRef]
75. Rahali, S.; Aissa, M.A.B.; Khezami, L.; Elamin, N.; Seydou, M.; Modwi, A. Adsorption behavior of Congo red onto barium-doped ZnO nanoparticles: Correlation between experimental results and DFT calculations. *Langmuir* **2021**, *37*, 7285–7294. [CrossRef]
76. Benhabiles, M.S.; Salah, R.; Lounici, H.; Drouiche, N.; Goosen, M.F.A.; Mameri, N. Antibacterial activity of chitin, chitosan and its oligomers prepared from shrimp shell waste. *Food Hydrocoll.* **2012**, *29*, 48–56. [CrossRef]
77. Seghir, B.B.; Benhamza, M.H. Preparation, optimization, and characterization of chitosan polymer from shrimp shells. *J. Food Meas. Charact.* **2017**, *11*, 1137–1147. [CrossRef]
78. Pokhrel, S.; Yadav, P.N. Functionalization of chitosan polymer and their applications. *J. Macromol. Sci. Pt. A* **2019**, *56*, 450–475. [CrossRef]
79. Li, X.; Zhou, H.; Wu, W.; Wei, S.; Xu, Y.; Kuang, Y. Studies of heavy metal ion adsorption on Chitosan/Sulfydryl-functionalized graphene oxide composites. *J. Colloid Interface Sci.* **2015**, *448*, 389–397. [CrossRef] [PubMed]
80. Motaharian, A.; Hosseini, M.R.M. Electrochemical sensor based on a carbon paste electrode modified by graphene nanosheets and molecularly imprinted polymer nanoparticles for determination of a chlordiazepoxide drug. *Anal. Methods* **2016**, *8*, 6305–6312. [CrossRef]
81. Sabnis, S.; Block, L.H. Improved infrared spectroscopic method for the analysis of degree of N-deacetylation of chitosan. *Polym. Bull.* **1997**, *39*, 67–71. [CrossRef]
82. Baxter, A.; Dillon, M.; Taylor, K.D.A.; Roberts, G.A.F. Improved method for i.r. determination of the degree of N-acetylation of chitosan. *Int. J. Biol. Macromol.* **1992**, *14*, 166–169. [CrossRef]
83. Kumari, S.; Rath, P.; Kumar, A.S.H.; Tiwari, T.N. Extraction and characterization of chitin and chitosan from fishery waste by chemical method. *Environ. Technol. Innov.* **2015**, *3*, 77–85. [CrossRef]
84. Rinaudo, M.; Milas, M.; Le Dung, P. Characterization of chitosan. Influence of ionic strength and degree of acetylation on chain expansion. *Int. J. Biol. Macromol.* **1993**, *15*, 281–285. [CrossRef]
85. Li, X.A.; Zhou, D.M.; Xu, J.J.; Chen, H.Y. In-channel indirect amperometric detection of heavy metal ions for electrophoresis on a poly(dimethylsiloxane) microchip. *Talanta* **2007**, *71*, 1130–1135. [CrossRef]
86. Majid, S.; El Rhazi, M.E.; Amine, A.; Curulli, A.; Palleschi, G. Carbon paste electrode bulk-modified with the conducting polymer Poly(1,8-Diaminonaphthalene): Application to lead determination. *Microchim. Acta* **2003**, *143*, 195–204. [CrossRef]
87. Senthilkumar, S.; Saraswathi, R. Electrochemical sensing of cadmium and lead ions at zeolite-modified electrodes: Optimization and field measurements. *Sens. Actuators B* **2009**, *141*, 65–75. [CrossRef]
88. Hwang, G.H.; Han, W.K.; Park, J.S.; Kang, S.G. An electrochemical sensor based on the reduction of screen-printed bismuth oxide for the determination of trace lead and cadmium. *Sens. Actuators B* **2008**, *135*, 309–316. [CrossRef]
89. Sebez, B.; Ogorevc, B.; Hocevar, S.B.; Veber, M. Functioning of antimony film electrode in acid media under cyclic and anodic stripping voltammetry conditions. *Anal. Chim. Acta* **2013**, *785*, 43–49. [CrossRef] [PubMed]
90. Kresse, G.; Hafner, J. Ab initio molecular dynamics for liquid metals. *Phys. Rev. B* **1993**, *47*, 558. [CrossRef]
91. Perdew, J.P.; Burke, K.; Ernzerhof, M. Generalized gradient approximation made simple. *Phys. Rev. Lett.* **1996**, *77*, 3865. [CrossRef]
92. Grimme, S.; Antony, J.; Ehrlich, S.; Krieg, H. A consistent and accurate ab initio parametrization of density functional dispersion correction (DFT-D) for the 94 elements H-Pu. *J. Chem. Phys.* **2010**, *132*, 154104. [CrossRef]